Article

Force Dependence of Proteins' Transition State Position and the Bell–Evans Model

Marc Rico-Pasto [1],[†] , Annamaria Zaltron [2],[†] and Felix Ritort [1],[*]

[1] Small Biosystems Lab, Condensed Matter Physics Department, Universitat de Barcelona,
   Carrer de Martí i Franquès 1, 08028 Barcelona, Spain; mricopasto@ub.edu
[2] Department of Physics and Astronomy, University of Padova, Via Marzolo 8, 35131 Padova, Italy;
   annamaria.zaltron@unipd.it
[*] Correspondence: ritort@ub.edu
[†] These authors contributed equally to this work.

Abstract: Single-molecule force spectroscopy has opened a new field of research in molecular biophysics and biochemistry. Pulling experiments on individual proteins permit us to monitor conformational transitions with high temporal resolution and measure their free energy landscape. The force–extension curves of single proteins often present large hysteresis, with unfolding forces that are higher than refolding ones. Therefore, the high energy of the transition state (TS) in these molecules precludes kinetic rates measurements in equilibrium hopping experiments. In irreversible pulling experiments, force-dependent kinetic rates measurements show a systematic discrepancy between the sum of the folding and unfolding TS distances derived by the kinetic Bell–Evans model and the full molecular extension predicted by elastic models. Here, we show that this discrepancy originates from the force-induced movement of TS. Specifically, we investigate the highly kinetically stable protein barnase, using pulling experiments and the Bell–Evans model to characterize the position of its kinetic barrier. Experimental results show that while the TS stays at a roughly constant distance relative to the native state, it shifts with force relative to the unfolded state. Interestingly, a conversion of the protein extension into amino acid units shows that the TS position follows the Leffler–Hammond postulate: the higher the force, the lower the number of unzipped amino acids relative to the native state. The results are compared with the quasi-reversible unfolding–folding of a short DNA hairpin.

Keywords: single-molecule force spectroscopy; protein folding; free-energy landscape; Bell–Evans model

1. Introduction

A prominent question in biophysics is how biomolecules, and particularly proteins, fold. At present, two debated theories on protein folding are based on the energy landscape and foldon hypotheses [1–4]. The first describes protein folding as a thermally activated relaxation process in a funneled energy landscape with the native state at the bottom of the funnel [1,2]. The funnel is rugged with deep valleys leading to intermediate states of short lifetime, where the polypeptide chain is partially folded. In the funnel model there are different trajectories for protein folding passing through one or more intermediates. In the late '80s, bulk hydrogen exchange, NMR, and mass spectrometry studies and theoretical models consistently observed recurrent intermediates during folding [5–8]. Based on these results, the foldon hypothesis claims that proteins fold along a unique path in the energy landscape connecting the native and unfolded state through several foldons [3,4].

Single-molecule techniques have emerged to investigate the thermodynamics of individual proteins with high temporal resolution [9,10]. Force spectroscopy techniques such as Atomic Force Spectroscopy, Magnetic and Optical Tweezers have significantly contributed in achieving new insights into this research area [11,12]. Specifically, these methods use force as a "denaturant agent" to mechanically break the bonds that stabilize the protein

structure [13]. The force is applied to the N- and C- termini of the polypeptide chain, defining a proper reaction coordinate, the end-to-end distance or molecular extension, useful to describe the folding free energy landscape (mFEL) [14–16]. Over the years, single-molecule experiments have permitted the reconstruction of the free energy landscape of a wide variety of proteins, both characterized by a two-state folding/unfolding process [15,17–19] and in the presence of intermediates [14,20–23].

In single-molecule experiments, the mFEL is widely investigated employing the phenomenological Bell–Evans model [24–27]. For a two-state system, the mFEL consists of two wells representing the native (N) and the denatured (or unfolded, U) states separated by a kinetic barrier placed at the transition state (TS) (Figure 1a). The Bell–Evans (BE) model assumes that the position of the barrier relative to N ($x^\dagger$) and U (x^*) is fixed. In contrast, its height relative to N (U) is reduced (increased) upon increasing the applied force in a linear fashion. Moreover, the unfolding and folding kinetic rates, $k_\rightarrow$ and $k_\leftarrow$, vary exponentially with the activation energies of the system and, as a result, are force-dependent. The BE model is often used to interpret the data derived either by equilibrium hopping experiments and non-equilibrium pulling experiments.

Hopping experiments are used to derive $k_\rightarrow$ and $k_\leftarrow$ from equilibrium force-time traces by determining the average lifetimes at each state [28–30]. These experiments provide good estimations for the molecular extension, $x_m = x^\dagger + x^*$, and the coexistence force f_c (where $k_\rightarrow(f_c) = k_\leftarrow(f_c)$) for molecules with lifetimes that fall in the experimentally accessible timescales, a requirement often met in DNA molecules but not in proteins. The difference arises from the large kinetic stability induced by protein tertiary structure. In fact, proteins typically refold at low forces, where molecular conformational transitions are hardly detectable, or are characterized by pronounced hysteresis. Therefore, unfolding and folding events occur in different force ranges, rendering hopping unobservable in experimental times. One might extract kinetic rates from force jump protocols, however these experiments can be inaccurate if the unfolding and folding transitions after the jump occur too fast. In such cases, non-equilibrium pulling experiments are useful to derive the kinetic rates from the survival probabilities of N and U, along the unfolding and folding trajectories, respectively [31–34]. Indeed, in these experiments, the large molecular folding timescales do not impede measurements of $k_\rightarrow$ and $k_\leftarrow$ at different forces. Thus, they can be used to investigate also proteins with high kinetic stability.

It has been shown that the molecular extension x_m derived from the BE model systematically underestimates the predictions based on the elastic properties of proteins [20,31,33]. Thus, the question arises about how to study kinetically stable proteins by combining pulling experiments with the BE model. Therefore, we analyze the unfolding/folding kinetic rates of barnase at room temperature (298 K), a two-state protein that has been shown to present pronounced hysteresis upon mechanical folding and unfolding with optical tweezers [33]. Barnase is a good candidate to test the BE model's success and limitations to reproduce the folding kinetics in mechanical unzipping experiments. To this aim, we compare the results for barnase with those relative to a reversible folder, such as a DNA hairpin [35–37], which kinetics can be measured in hopping experiments. We find that the sum of $x^\dagger$ and x^* derived from pulling experiments underestimates the expected full molecular extension of the protein, x_m. However, a conversion of transition state distances into amino acid units permits us to recover the protein extension correctly and, more interestingly, to derive the force dependent folding rates and the coexistence force in the inaccessible intermediate force range. Results are also interpreted in the light of the Leffler–Hammond postulate [38,39].
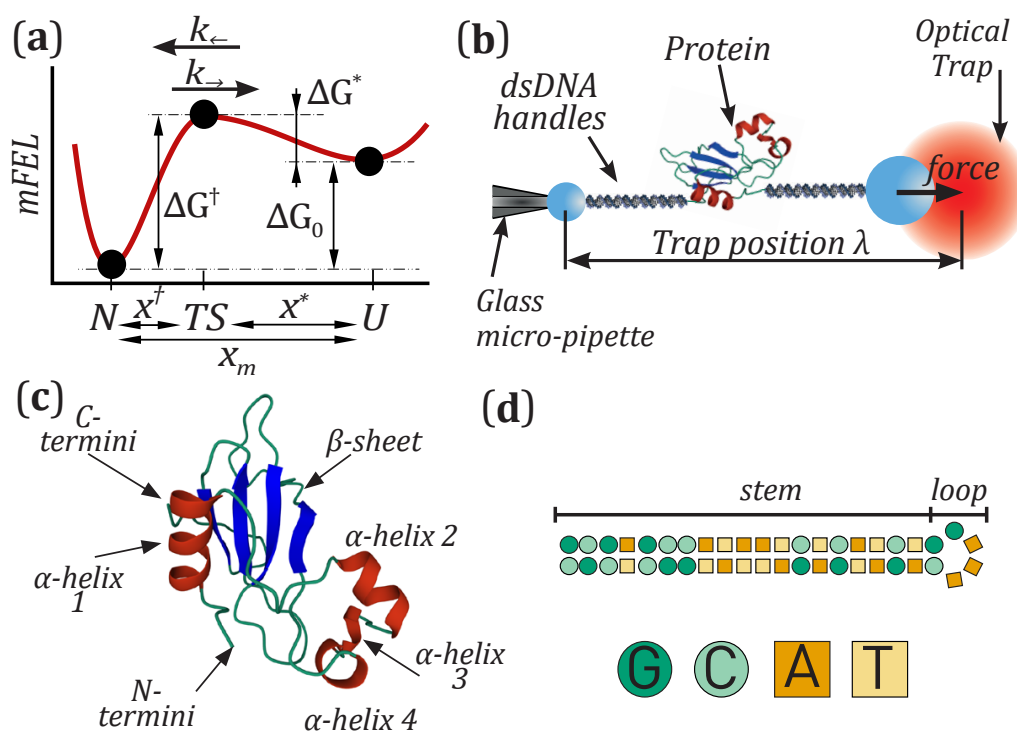
Figure 1. Single-molecule experiments. (**a**) Illustration of the mFEL of barnase. A kinetic barrier (located at the transition state TS) mediates transitions between N and U. ΔG_0 is the free energy difference between N and U, whereas $\Delta G^\dagger$ and ΔG^* are the kinetic barriers relative to N and U, respectively. (**b**) Illustration of the single-molecule experimental setup. The optical trap measures the force f applied to the ends of the molecular construct. The distance between the optical trap and the pipette, λ, denotes the control parameter of the experiment. (**c**) Structure of the protein barnase [40]. (**d**) Sequence of the DNA hairpin [35].

2. Materials and Methods

2.1. Molecular Synthesis

In single-molecule experiments with optical tweezers, the molecule under investigation is tethered between two beads via double-stranded DNA handles (Figure 1b). The use of DNA handles avoids undesired interactions between the molecule and the beads during the measurements. The molecular construct is connected to two polystyrene beads via specific linkages. The free ends of the DNA handles are labeled with a biotin and a digoxigenin, that bind to beads specifically coated with streptavidin (SA; 2.0–2.9-µm-diameter bead; G. Kisker Biotech, Steinfurt, Germany) and anti-digoxigenin (AD; 3.0–3.4-µm-diameter bead; G. Kisker Biotech, Steinfurt, Germany), respectively [41]. Barnase has been expressed as reported in [33]. It contains 110 amino acids (Figure 1c) and folds forming four external α-helices surrounding a β-sheet [40]; its N- and C-termini have been modified with cysteine-thiol groups that act as anchoring points for the two 500 bp dsDNA handles. Finally, the DNA hairpin has been synthesised as described in [35] and it contains 44 nucleotides that form a 20 bp stem ending in a tetraloop (Figure 1d).

2.2. Optical Tweezers Setup

The mini-tweezers instrument has been described in [42]. It consists of two counter-propagating laser beams (845 nm) that pass through two microscope objectives (Olympus x60, NA 1.2) forming a single optical trap. The optical trap is moved with nanometric precision using piezoelectric actuators (Thorlabs Inc., Newton, NJ, USA). The experiments are carried out by moving the AD bead captured in the optical trap relative to the SA bead, which is kept fixed at the tip of a glass micro-pipette (King Precision Glass Inc., Claremont, CA, USA) by air suction (Figure 1b). In this way, an external force is applied to the protein or DNA

hairpin tethered between the beads. The instrument records the force and trap position in real-time. Pulling and hopping experiments are carried out at high temporal (1 kHz) and nanometer spatial resolution [43].

3. Results

3.1. Unfolding and Folding Kinetic Rates

We present kinetic rate measurements from pulling experiments on protein barnase, as reported in [33]. We compare them with results from DNA hairpins presented in [35,37]. The kinetics of DNA hairpins has been measured in equilibrium hopping experiments in the passive mode (see Figure 2a). In these experiments, transitions between different states are monitored while maintaining fixed (clamped) the trap–pipette distance. The kinetic rates are derived from the mean lifetimes of the unfolded and folded states [44], which have been measured at different trap positions to reconstruct their force dependence. Hopping experiments are widely used in short DNA/RNA hairpins (few tens of base-pairs), since the majority of these molecules fold and unfold in the second and subsecond timescales [37,45] (Figure 2a). Hopping experiments have been also carried out to study conformational transitions in proteins triggered by the reorganization of small domains, e.g., in [14,20,46–48]. Still, the folding kinetics of sufficiently large proteins (above a few tens of amino acids) remains inaccessible in hopping experiments, making non-equilibrium pulling experiments particularly advantageous.
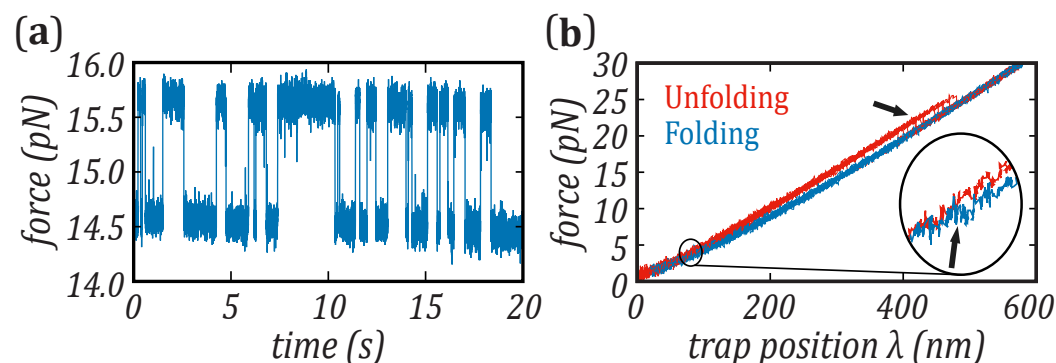

Figure 2. Single-molecule experiments on a DNA hairpin and protein barnase. (**a**) Equilibrium hopping experiments in the 20 bp DNA hairpin of Figure 1d: selected trace at the coexistence force (∼15 pN). (**b**) Non-equilibrium pulling experiments on barnase protein. The unfolding (red) and folding (blue) curves present hysteresis, with the folding events occurring at very low forces (below 5 pN).

In the pulling experiments carried out in this work, the optical trap is repeatedly moved back and forth at a constant loading rate, $r = 6$ pN/s. The force and position are measured, generating the force–distance curves (FDCs) shown in Figure 2b. The protein is pulled from an initial force, ∼1 pN, where it is in N, to a final force, ∼30 pN, where it is in U, producing unfolding trajectories (red curves in Figure 2b). The unfolding events are observed as sudden force drops in the FDCs (black arrow in Figure 2b, main). When force is relaxed (folding trajectories, blue curve in Figure 2b), the protein folds into N and the event is observed as a sudden force increase of about 0.5 pN at lower forces, <5 pN (black arrow in the enlarged region of Figure 2b). In [33], it has been shown that the molecular extension upon barnase unfolding corresponds to the release of the 110aa of the native structure, proving that barnase always folds into N in the refolding process. To determine the folding events down to forces as low as 1 pN we used a median-filter applied to the unfolding and folding trajectories. The folded branch can be fitted to a linear function, $f(\lambda) = k\lambda$, with k being the effective stiffness of the optical trap plus molecular construct. We used this fit to build a reference folded-baseline by subtracting the folded force branch to the linear fit. The Gaussian distribution of forces along the folded-baseline and a Bayesian method are used to classify into N and U the median-filtered data points along a given folding

trajectory. The folding force is defined as the point along the folding trajectory in which the transition $U \rightarrow N$ is observed. Even if we can detect folding events below 2 pN, we do not detect all of them. For this reason, we have not included in Figure 3c the force points below 2 pN.
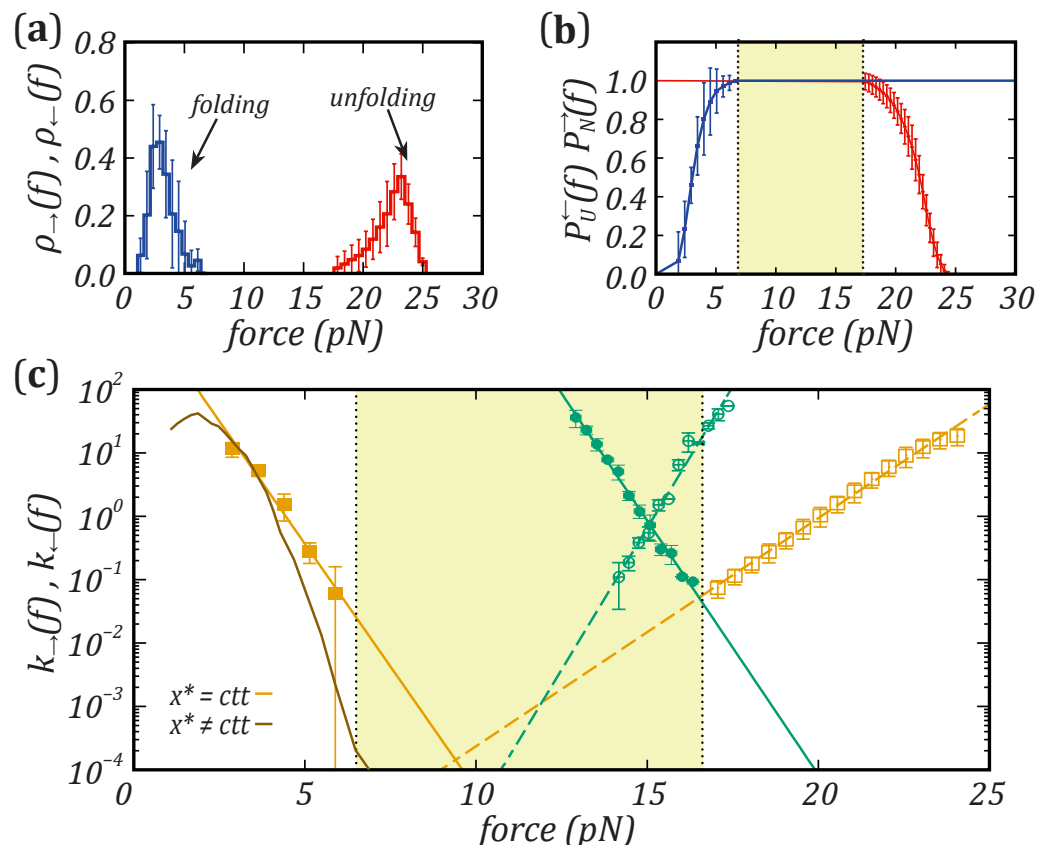

Figure 3. Pulling experiments in barnase at room temperature (298 K). (**a**) Barnase unfolding and folding force distributions. (**b**) Survival probabilities of the folded ($P_U^{\leftarrow}(f)$, red symbols) and unfolded ($P_N^{\rightarrow}(f)$, blue symbols) states. (**c**) Average unfolding (empty symbols) and folding (solid symbols) kinetic rates of the DNA hairpin (green) and barnase (yellow). The yellow area highlights the wide range of forces were the kinetic rates of barnase can not be measured. The yellow and green lines are the fits of the kinetic rates to the BE model; the brown line represents the estimation of the folding kinetic rates of barnase, assuming a movement of the TS position with respect to the unfolded state, x^*, as discussed in Section 3.2 and shown in Figure 4b.

From the force–distance curves, we extract the rupture force distributions $\rho_{\rightarrow}(f)$ and $\rho_{\leftarrow}(f)$ of the first unfolding and folding events, as reported in Figure 3a for a selected molecule. The plots clearly show that the mechanical folding/unfolding of barnase is highly irreversible, with separated ($\sim$10 pN) unfolding and folding force distributions. The large hysteresis impedes to extract kinetic rates $k_{\rightarrow}$ and $k_{\leftarrow}$ by doing hopping experiments, due to the disparity of lifetimes of states N and U. Unfolding and folding kinetic rates of barnase can be derived from pulling experiments by measuring the survival probabilities of states N and U, $P_N^{\rightarrow}(f)$ and $P_U^{\leftarrow}(f)$. These are given by

$$P_N^{\rightarrow}(f) = 1 - \int_{f_{min}}^{f} \rho_{\rightarrow}(f')df'$$

$$P_U^{\leftarrow}(f) = 1 - \int_{f}^{f_{max}} \rho_{\leftarrow}(f')df'$$

(1)

where f_{min} and f_{max} denote the minimum and maximum forces (for simplicity we can take them as $-\infty$ and ∞, respectively). Figure 3b shows the survival probabilities $P_N^\rightarrow(f)$ and $P_U^\leftarrow(f)$ of protein barnase at 25 °C, where the high irreversibility of its mechanical folding is evidenced. In fact, $P_N^\rightarrow(f)$ and $P_U^\leftarrow(f)$ do not cross in the investigated force range (highlighted area in Figure 3b). Finally, by modeling the unfolding and folding kinetics as a first-order Markov process, kinetic rates can be calculated from the rupture force distributions as [49]

$$\rho_\rightarrow(f) = \frac{k_\rightarrow(f)}{r} P_N^\rightarrow(f) \;\Rightarrow\; k_\rightarrow(f) = r\frac{\rho_\rightarrow(f)}{P_N(f)} \tag{2}$$

$$\rho_\leftarrow(f) = \frac{k_\leftarrow(f)}{r} P_U^\leftarrow(f) \;\Rightarrow\; k_\leftarrow(f) = r\frac{\rho_\leftarrow(f)}{P_U^\leftarrow(f)} \tag{3}$$

where $r = |df/dt|$ is the constant loading and unloading rate. The results are shown in a log-normal plot in Figure 3c (yellow symbols), where kinetic rates for the DNA hairpin have been also reported for comparison (green symbols). In this case, folding and unfolding kinetic rates span a narrow range of forces (~13–17 pN), around the coexistence force (~15 pN). In contrast, the yellow area highlights the force range where kinetic measurements from equilibrium hopping experiments are not feasible for barnase. Kinetic rates of the DNA hairpin and barnase present a linear force-dependence, which is discussed in the next section.

3.2. The Transition State Position and the Leffler–Hammond Postulate

The force dependence of the folding and unfolding kinetic rates is well approximated by the BE model. In this model, the height of the barrier located at the *TS* linearly decreases with the applied force f. The decrease rate equals the distances of the *TS* to the native and denatured states ($x^\dagger$ and x^*) which are taken as constant. The BE kinetic rates are given by

$$k_\rightarrow(f) = k_a \exp\left(-\beta\Delta G^\dagger\right) \exp\left(\beta f x^\dagger\right) \tag{4}$$

$$k_\leftarrow(f) = k_a \exp\left(-\beta\Delta G^*\right) \exp\left(\beta\left(\Delta G_0 - f x^*\right)\right) \tag{5}$$

where ΔG_0 is the free energy difference between N and U, $\Delta G^\dagger$ and ΔG^* are the barrier's heights relative to N and U (see Figure 1a), $\beta = 1/k_B T$ (with k_B the Boltzmann constant and T the temperature), and k_a is the attempt rate, which depends on the experimental conditions.

By fitting Equations (4) and (5) to the experimental values of $k_\rightarrow(f)$ and $k_\leftarrow(f)$ (dashed and solid lines in Figure 3c), we derive the position and the height of the energetic barriers. First, the values that best fit the BE model to the experimental data have been used to estimate the coexistence force for barnase $f_c = (9.0 \pm 0.5)$ pN, where $k_\rightarrow(f_c) = k_\leftarrow(f_c)$. The error in the estimate includes the systematic error in force calibration which is about 5%. N and U have the same free energy at the coexistence force, meaning that the barriers to unfold or fold the protein are the same. Second, we have carried out an in-depth analysis about the position of the kinetic barrier. From the fits to the kinetic rates, we have derived $x^\dagger$ and x^*. The errors of $x^\dagger$ and x^* have been calculated as the standard statistical error taken from the values taken over all five studied molecules, giving $x^\dagger = (3 \pm 1)$ nm and $x^* = (8 \pm 1)$ nm, which sum $x_{m,exp} = x^\dagger + x^* = (11 \pm 2)$ nm. In the BE model, the latter should be equal to the full molecular extension of the protein at the coexistence force. In the following, we show that $x_{m,exp} = (11 \pm 2)$ nm largely underestimates the value predicted from the elastic theory of polymers. This indicates that the assumption that $x^\dagger, x^*$ are force-independent does not hold. Moreover, in [33], the unfolding and folding kinetic rates have been studied with the Dudko–Hummer–Szabo (DHS) model [50]. This model is parametrized by a parameter γ that interpolates between different TS shapes (BE corresponding to $\gamma = 1$) finding $x_{m,exp} = (10 \pm 2)$ nm for a parabolic shape ($\gamma = 1/2$) and $x_{m,exp} = (10 \pm 1)$ nm for a cubic shape ($\gamma = 2/3$), whereas for the BE model we get

$x_{m,exp} = (11 \pm 2)$ nm. Considering the expected value from the inextensible Worm-Like Chain (WLC) prediction, $x_{m,th} = (21 \pm 1)$ nm, the above results show that both BE and DHS largely underestimate the full molecular extension.

To derive the theoretical prediction for $x_{m,th}(f)$, we have calculated the extension of the polypeptide chain released upon unfolding at a given force f, $X(f)$. To $X(f)$ we must subtract the protein elongation in the native state just before the rip, $x_d(f)$, which gives $x_{m,th}(f) = X(f) - x_d(f)$. The initial extension of the folded protein, $x_d(f)$, is modeled as a dipole of length equal to the N-C-termini distance (3 nm for barnase [33,40]). The dipole orients under an applied force, its average extension being equivalent to that of a single Kühn segment (in the Freely Jointed Chain (FJC) model) of length equal to that of the dipole (3 nm). Besides, the value of $X(f)$ is determined by using the inextensible Worm-Like Chain (WLC) model and its interpolation formula between high and low forces [51,52]

$$f = \frac{k_B T}{4L_p} \left[\left(1 - \frac{X(f)}{Nd_{aa}} \right)^{-2} + 4\frac{X(f)}{Nd_{aa}} - 1 \right] \qquad (6)$$

where $L_p = 0.8$ nm is the persistence length of the polypeptide chain, N is the number of residues (110 for barnase [33]), and $d_{aa} = 0.37$ nm is the aa distance [33]. Using these elastic parameters, the theoretical molecular extension at f_c is $x_{m,th}(f_c) = X(f_c) - x_d(f_c) = (21 \pm 1)$ nm, which differs by ~ 9 nm from the value derived from the BE model, $x_{m,exp} = (11 \pm 2)$ nm. This discrepancy arises from the strong hysteresis between unfolding and folding and the different range of forces used to measure $x^\dagger$ and x^*. Indeed, fits of $k_\rightarrow$ and $k_\leftarrow$ to the BE model are made close to the most probable unfolding and refolding forces, meaning that the values of $x^\dagger$ and x^* are estimated at very different forces, far from f_c. In contrast, the expected molecular extension has been calculated from the elastic models at f_c. Therefore, to properly compare the measured values $x^\dagger$ and x^* with the theoretical prediction, these must be estimated at the same force. In the DNA hairpin, both unfolding and folding kinetic rates have been measured in the same force range close to $f_{c,DNA} \sim 15$ pN. As a consequence, the DNA extension theoretically predicted by the WLC model, $x_{DNA,th} = (18.0 \pm 0.3)$ nm (with L_p, d_{aa} and x_d given in [52,53]) matches that obtained from the BE model ($x_{DNA,exp} = (17.9 \pm 0.4)$ nm). The number of released bases at the transition state at f_c are $n^\dagger = 20 \pm 1$ and $n^* = 23 \pm 2$, which sum gives the total 44 bases of the hairpin.

To estimate the TS position of barnase, we have converted barrier distances $x^\dagger$ and x^* into the number of unfolded amino acids relative to N ($n_{aa}^\dagger$) and U (n_{aa}^*), by using the WLC model, Equation (6). The obtained values at the most probable unfolding and folding forces are $n_{aa}^\dagger = (13 \pm 1)$aa and $n_{aa}^* = (69 \pm 3)$aa, which sum $n_{aa}^\dagger + n_{aa}^* \simeq 82$ underestimates the full number of amino acids (110).

This result could indicate the presence of intermediate states in the unfolding/folding pathway. However, calorimetric studies [54,55] and numerical simulations [56] have previously demonstrated that barnase folds in a two-state manner. A plausible explanation of the discrepancy is that the distances to the TS (expressed in amino acid units) are not fixed but change with force. In fact, upon increasing the force, the extension of that part of the polypeptide chain that is unfolded at TS (which contains $n_{aa}^\dagger$ aa) should increase as predicted by Equation (6). At the same time, $n_{aa}^\dagger$ decreases with force as predicted by the Leffler–Hammond postulate for chemical reactions [38,39]. According to this postulate, upon applying an external perturbation (e.g., force), the TS position moves toward N (U) to counteract the increased thermodynamic stability of the U (N) state. Upon stretching, the postulate predicts that the number of released (adsorbed) amino acids in the TS during unfolding (folding), $n_{aa}^\dagger$ (n_{aa}^*), decreases (increases) with force. In the unfolding case, a compensation between the two effects leads to a $N - TS$ extension $x^\dagger$ which is roughly constant, explaining the linearity of the $\log(k_\rightarrow)$ versus force observed in Figure 3c in the range 16–23 pN (yellow dashed line). In contrast, such linearity is not expected for the folding rate ($\log(k_\rightarrow)$ versus force). Upon increasing the force, n_{aa}^* increases with force, therefore no compensation occurs between such increase and that of the molecular extension, x^*.

To verify this, we have used the WLC model (Equation (6)) to calculate $n_{aa}^\dagger$ over the full range of forces, assuming a constant value of $x^\dagger$. The results are reported in Figure 4a and show that $n_{aa}^\dagger$ decreases when the force increases, in agreement with the Leffler–Hammond postulate. Then, we used the value of $n_{aa}^\dagger$ estimated at the most probable folding force $\langle f_\leftarrow \rangle = (3.0 \pm 0.2)\,$pN to sum it with the value of n_{aa}^* obtained from the folding kinetic rates and the WLC model. At $\langle f_\leftarrow \rangle$, the protein extension in amino acids is $n_{aa}^{tot} = n_{aa}^\dagger + n_{aa}^* = (37 \pm 1) + (69 \pm 3)\text{aa} = 106 \pm 4\text{aa}$, a result compatible with the 110 amino acids of barnase. This result confirms the two-state behavior of barnase folding and, above all, the effective movement of the transition state which occurs to counteract the action of the force. The compensation between the change in $n_{aa}^\dagger$ and the molecular extension with force in (6), reported at forces as low as $\langle f_\leftarrow \rangle = (3.0 \pm 0.2)\,$pN shows that the linear behavior of $\log(k_\rightarrow)$ versus f leads to an approximately constant value of $x^\dagger$ throughout the whole range of forces. Probably this compensation is just casual, in fact a constant $x^\dagger$ is not always observed, e.g., in DNA and RNA hairpins [57–59].

From $n_{aa}^\dagger(f)$ we extract $n_{aa}^*(f)$ by subtracting $n_{aa}^\dagger(f)$ to the total number of amino acids (110), $n_{aa}^*(f) = 110 - n_{aa}^\dagger(f)$. Figure 4a shows that $n_{aa}^*(f)$ exhibits a force dependence opposite to that of $n_{aa}^\dagger$, approaching U as force decreases. In Figure 4b, we show $x^*(f)$, derived by using Equation (6) and the values of n_{aa}^* reported in Figure 4a. In contrast to $x^\dagger$, x^* presents a strong force dependence. Its value increases up to $\sim$30 nm at the maximum unfolding force ($\sim$25 pN). Another interesting quantity is the mechanical fragility of barnase, defined as $\mu(f) = (x^\dagger - x^*)/x_m$, where $x_m = x^\dagger + x^*$. In Figure 4c we show the fragility as a function of force. The Leffler–Hammond postulate predicts that the fragility is a monotonically decreasing function of force [59], with compliant unfolding at low forces and brittle unfolding at high forces.
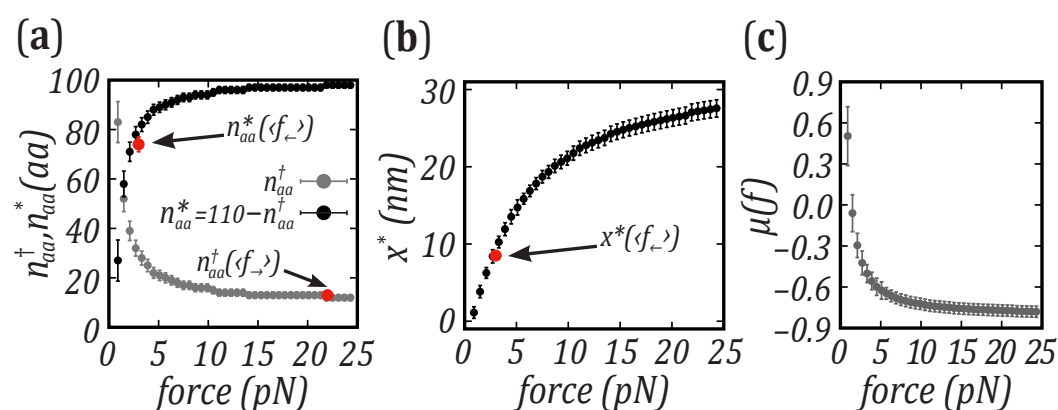

Figure 4. Force-dependent *TS* position. (**a**) Number of released and absorbed amino acids at *TS* relative to N, $n_{aa}^\dagger$ (gray), and U, n_{aa}^* (black), respectively. The force dependence of $n_{aa}^\dagger$ is evaluated assuming a constant $x^\dagger$ and using the WLC model; the values of n_{aa}^* are calculated as $110 - n_{aa}^\dagger$. The red circles show the values of $n_{aa}^\dagger$ and n_{aa}^* calculated at the most probable unfolding and refolding forces, by fitting the BE model to the experimental kinetic rates. (**b**) *TS* position relative to U, x^*, versus force. The values of x^* are derived by using Equation (6) and the values of n_{aa}^* reported in (**a**). The red circle represents the value of x^* calculated at the most probable folding force, by using the experimental folding kinetic rates. (**c**) Fragility of barnase versus force.

4. Discussion

In this work, we have investigated the effect of force on the molecular free energy landscape (mFEL) of protein barnase. Barnase is a suitable model due to its high mechanical stability showing large hysteresis in the FDCs [33]. Barnase also shows a two-state folding, in bulk experiments [54,55] and simulations [56]. In particular, we address the question of the reported underestimation of the molecular extension when the BE model is used to fit the force-dependent kinetic rates [14,29,32].

To this end, we have analyzed non-equilibrium pulling data to extract the force-dependent unfolding and folding kinetic rates ($k_\rightarrow$ and $k_\leftarrow$) at room temperature. The distances of the transition state (TS) to the native (N) and unfolded (U) states, $x^\dagger$ and x^*, have been calculated from the force-dependent kinetic rates using the BE model. The experimentally derived sum $x^\dagger + x^*$ underestimates the total molecular extension x_m calculated from the elastic worm-like chain (WLC) model. To resolve this discrepancy, we derived the number of released amino acids at the TS, $n_{aa}^\dagger$, from the extensions $x^\dagger$ using the WLC model. We have found that the TS position approaches N upon increasing the force, while $x^\dagger$ remains approximately constant as assumed in the BE model. This result agrees with the Leffler–Hammond postulate, which states that in chemical reactions the TS moves toward the reactants when an external agent favors the products [38,39]. Nuclear Magnetic Resonance (NMR) spectroscopy experiments in the early '90s confirmed the validity of this postulate using engineered mutants to modify the thermodynamic stability of barnase [60]. Our results confirm that force is a very efficient denaturant, capable of inducing a movement of the TS. The results of Figure 4a confirm that $x^\dagger(f)$ is roughly constant due to the compensation between the decrease of $n_{aa}^\dagger(f)$ and the increase of the molecular extension per aa, ($x_{1aa}^\dagger(f)$) with force f, or $x^\dagger(f) = n_{aa}^\dagger(f)x_{1aa}^\dagger(f) \simeq$ cnst. In contrast, such compensation does not occur for $x^*(f)$ which markedly changes with force (Figure 4b), predicting a curvature in the $\log(k_\leftarrow)$ versus f plots (Figure 3c, brown line). Yet, the curvature observed in the data (filled squares in Figure 3c), is smaller than that predicted from $x^*(f)$ in Figure 4b. This discrepancy indicates that the assumption of a constant $x^\dagger(f)$ is only an approximation that might be refined by matching the measured and predicted values of $k_\leftarrow(f)$.

Finally, one might ask about the biological significance of the variation of $n_{aa}^\dagger$ with force reported in Figure 4, which shows a marked decrease below 5 pN. This result might indicate a regulatory role of force in a wide variety of biological processes governed by conformational changes of proteins. Our results confirm the general validity of the BE model to investigate the kinetics and mFEL of highly kinetically stable proteins. The analysis based on the movement of the TS position paves the way for future studies on other proteins with a mechanical role, such as scleroproteins [61], metalloproteins that bind to metal ions [62] or lipoproteins, which are transient intermediates in the process of lipids' transfer [63].

Author Contributions: Conceptualization, M.R.-P., A.Z. and F.R.; Data curation, M.R.-P.; Funding acquisition, A.Z. and F.R.; Investigation, M.R.-P. and A.Z.; Supervision, F.R.; Visualization, M.R.-P.; Writing—original draft, M.R.-P. and A.Z.; Writing—review and editing, A.Z. and F.R. All authors have read and agreed to the published version of the manuscript.

Data Availability Statement: The data presented in this study are available on request from the corresponding author.

Conflicts of Interest: The authors declare no conflict of interest.

References

1. Frauenfelder, H.; Sligar, S.; Wolynes, P. The energy landscapes and motions of proteins. *Science* **1991**, *254*, 1598–1603. [CrossRef]
2. Bryngelson, J.D.; Onuchic, J.N.; Socci, N.D.; Wolynes, P.G. Funnels, pathways, and the energy landscape of protein folding: A synthesis. *Proteins Struct. Funct. Bioinform.* **1995**, *21*, 167–195. [CrossRef]
3. Baldwin, R.L. The nature of protein folding pathways: The classical versus the new view. *J. Biomol. NMR* **1995**, *5*, 103–109. [CrossRef]
4. Maity, H.; Maity, M.; Krishna, M.M.G.; Mayne, L.; Englander, S.W. Protein folding: The stepwise assembly of foldon units. *Proc. Natl. Acad. Sci. USA* **2005**, *102*, 4741–4746. [CrossRef]

5. Camacho, C.J.; Thirumalai, D. Kinetics and thermodynamics of folding in model proteins. *Proc. Natl. Acad. Sci. USA* **1993**, *90*, 6369–6372. [CrossRef] [PubMed]

6. Shakhnovich, E.I. Proteins with selected sequences fold into unique native conformation. *Phys. Rev. Lett.* **1994**, *72*, 3907–3910. [CrossRef] [PubMed]

7. Chan, H.S.; Dill, K.A. Transition states and folding dynamics of proteins and heteropolymers. *J. Chem. Phys.* **1994**, *100*, 9238–9257. [CrossRef]

8. Bai, Y.; Sosnick, T.; Mayne, L.; Englander, S. Protein folding intermediates: Native-state hydrogen exchange. *Science* **1995**, *269*, 192–197. [CrossRef]

9. Rief, M.; Gautel, M.; Oesterhelt, F.; Fernandez, J.M.; Gaub, H.E. Reversible Unfolding of Individual Titin Immunoglobulin Domains by AFM. *Science* **1997**, *276*, 1109–1112. [CrossRef] [PubMed]

10. Kellermayer, M.S.Z.; Smith, S.B.; Granzier, H.L.; Bustamante, C. Folding-Unfolding Transitions in Single Titin Molecules Characterized with Laser Tweezers. *Science* **1997**, *276*, 1112–1116. [CrossRef] [PubMed]

11. Neumann, C.K.; Nagy, A. Single-molecule force spectroscopy: Optical tweezers, magnetic tweezers and atomic force microscopy. *Nat. Methods* **2008**, *5*, 491–505. [CrossRef]

12. Zaltron, A.; Merano, M.; Mistura, G.; Sada, C.; Seno, F. Optical tweezers in single-molecule experiments. *Eur. Phys. J. Plus* **2020**, *135*, 1–33. [CrossRef]

13. Bustamante, C.; Alexander, L.; Maciuba, K.; Kaiser, C.M. Single-Molecule Studies of Protein Folding with Optical Tweezers. *Annu. Rev. Biochem.* **2020**, *89*, 443–470. [CrossRef] [PubMed]

14. Gebhardt, J.C.M.; Bornschlögl, T.; Rief, M. Full distance-resolved folding energy landscape of one single protein molecule. *Proc. Natl. Acad. Sci. USA* **2010**, *107*, 2013–2018. [CrossRef] [PubMed]

15. Neupane, K.; Manuel, A.P.; Woodside, M.T. Protein folding trajectories can be described quantitatively by one-dimensional diffusion over measured energy landscapes. *Nat. Phys.* **2016**, *12*, 700–703. [CrossRef]

16. Rebane, A.A.; Ma, L.; Zhang, Y. Structure-Based Derivation of Protein Folding Intermediates and Energies from Optical Tweezers. *Biophys. J.* **2016**, *110*, 441–454. [CrossRef]

17. Sharma, D.; Perisic, O.; Peng, Q.; Cao, Y.; Lam, C.; Lu, H.; Li, H. Single-molecule force spectroscopy reveals a mechanically stable protein fold and the rational tuning of its mechanical stability. *Proc. Natl. Acad. Sci. USA* **2007**, *104*, 9278–9283. [CrossRef] [PubMed]

18. Zheng, P.; Wang, Y.; Li, H. Reversible Unfolding–Refolding of Rubredoxin: A Single-Molecule Force Spectroscopy Study. *Angew. Chem. Int. Ed.* **2014**, *53*, 14060–14063. [CrossRef]

19. Goldman, D.H.; Kaiser, C.M.; Milin, A.; Righini, M.; Tinoco, I.; Bustamante, C. Mechanical force releases nascent chain–mediated ribosome arrest in vitro and in vivo. *Science* **2015**, *348*, 457–460. [CrossRef]

20. Cecconi, C.; Shank, E.A.; Bustamante, C.; Marqusee, S. Direct Observation of the Three-State Folding of a Single Protein Molecule. *Science* **2005**, *309*, 2057–2060. [CrossRef] [PubMed]

21. Stigler, J.; Ziegler, F.; Gieseke, A.; Gebhardt, J.C.M.; Rief, M. The Complex Folding Network of Single Calmodulin Molecules. *Science* **2011**, *334*, 512–516. [CrossRef]

22. Stockmar, F.; Kobitski, A.Y.; Nienhaus, G.U. Fast Folding Dynamics of an Intermediate State in RNase H Measured by Single-Molecule FRET. *J. Phys. Chem. B* **2016**, *120*, 641–649. [CrossRef] [PubMed]

23. Yu, H.; Siewny, M.G.W.; Edwards, D.T.; Sanders, A.W.; Perkins, T.T. Hidden dynamics in the unfolding of individual bacteriorhodopsin proteins. *Science* **2017**, *355*, 945–950. [CrossRef]

24. Evans, E.; Ritchie, K. Dynamic strength of molecular adhesion bonds. *Biophys. J.* **1997**, *72*, 1541–1555. [CrossRef]

25. Bell, G.I. Models for the specific adhesion of cells to cells. *Science* **1978**, *200*, 618–627. [CrossRef] [PubMed]

26. Merkel, R.; Nassoy, P.; Leung, A.; Ritchie, K.; Evans, E. Energy landscapes of receptor–ligand bonds explored with dynamic force spectroscopy. *Nature* **1999**, *397*, 50. [CrossRef]

27. Evans, E. Probing the relation between force—Lifetime—And chemistry in single molecular bonds. *Annu. Rev. Biophys. Biomol. Struct.* **2001**, *30*, 105–128. [CrossRef]

28. Heidarsson, P.O.; Naqvi, M.M.; Otazo, M.R.; Mossa, A.; Kragelund, B.B.; Cecconi, C. Direct single-molecule observation of calcium-dependent misfolding in human neuronal calcium sensor-1. *Proc. Natl. Acad. Sci. USA* **2014**, *111*, 13069–13074. [CrossRef]

29. Jahn, M.; Tych, K.; Girstmair, H.; Steinmaßl, M.; Hugel, T.; Buchner, J.; Rief, M. Folding and Domain Interactions of Three Orthologs of Hsp90 Studied by Single-Molecule Force Spectroscopy. *Structure* **2018**, *26*, 96–105.e4. [CrossRef]

30. Mehlich, A.; Fang, J.; Pelz, B.; Li, H.; Stigler, J. Slow Transition Path Times Reveal a Complex Folding Barrier in a Designed Protein. *Front. Chem.* **2020**, *8*, 587824. [CrossRef]

31. Shank, E.A.; Cecconi, C.; Dill, J.W.; Marqusee, S.; Bustamante, C. The folding cooperativity of a protein is controlled by its chain topology. *Nature* **2010**, *465*, 637–640. [CrossRef]

32. Motlagh, H.N.; Toptygin, D.; Kaiser, C.M.; Hilser, V.J. Single-Molecule Chemo-Mechanical Spectroscopy Provides Structural Identity of Folding Intermediates. *Biophys. J.* **2016**, *110*, 1280–1290. [CrossRef]

33. Alemany, A.; Rey-Serra, B.; Frutos, S.; Cecconi, C.; Ritort, F. Mechanical Folding and Unfolding of Protein Barnase at the Single-Molecule Level. *Biophys. J.* **2016**, *110*, 63–74. [CrossRef]

34. Liu, K.; Chen, X.; Kaiser, C.M. Energetic dependencies dictate folding mechanism in a complex protein. *Proc. Natl. Acad. Sci. USA* **2019**, *116*, 25641–25648. [CrossRef] [PubMed]

35. Forns, N.; de Lorenzo, S.; Manosas, M.; Hayashi, K.; Huguet, J.; Ritort, F. Improving Signal/Noise Resolution in Single-Molecule Experiments Using Molecular Constructs with Short Handles. *Biophys. J.* **2011**, *100*, 1765–1774. [CrossRef]

36. Palassini, M.; Ritort, F. Improving free-energy estimates from unidirectional work measurements: Theory and experiment. *Phys. Rev. Lett.* **2011**, *107*, 060601. [CrossRef]

37. Rico-Pasto, M.; Pastor, I.; Ritort, F. Force feedback effects on single molecule hopping and pulling experiments. *J. Chem. Phys.* **2018**, *148*, 123327. [CrossRef]

38. Leffler, J.E. Parameters for the description of transition states. *Science* **1953**, *117*, 340–341. [CrossRef] [PubMed]

39. Hammond, G.S. A correlation of reaction rates. *J. Am. Chem. Soc.* **1955**, *77*, 334–338. [CrossRef]

40. Martin, C.; Richard, V.; Salem, M.; Hartley, R.; Mauguen, Y. Refinement and structural analysis of barnase at 1.5 Å resolution. *Acta Crystallogr. Sect. D* **1999**, *55*, 386–398. [CrossRef] [PubMed]

41. van der Sleen, L.M.; Tych, K.M. Bioconjugation Strategies for Connecting Proteins to DNA-Linkers for Single-Molecule Force-Based Experiments. *Nanomaterials* **2021**, *11*, 2424. [CrossRef]

42. Huguet, J.M.; Bizarro, C.V.; Forns, N.; Smith, S.B.; Bustamante, C.; Ritort, F. Single-molecule derivation of salt dependent base-pair free energies in DNA. *Proc. Natl. Acad. Sci. USA* **2010**, *107*, 15431–15436. [CrossRef]

43. de Lorenzo, S.; Ribezzi-Crivellari, M.; Arias-Gonzalez, J.R.; Smith, S.B.; Ritort, F. A Temperature-Jump Optical Trap for Single-Molecule Manipulation. *Biophys. J.* **2015**, *108*, 2854–2864. [CrossRef]

44. Li, P.T.X.; Collin, D.; Smith, S.B.; Bustamante, C.; Tinoco, I.J. Probing the Mechanical Folding Kinetics of TAR RNA by Hopping, Force-Jump, and Force-Ramp Methods. *Biophys. J.* **2006**, *130*, 250. [CrossRef]

45. Woodside, M.T.; Behnke-Parks, W.M.; Larizadeh, K.; Travers, K.; Herschlag, D.; Block, S.M. Nanomechanical measurements of the sequence-dependent folding landscapes of single nucleic acid hairpins. *Proc. Natl. Acad. Sci. USA* **2006**, *103*, 6190–6195. [CrossRef]

46. Gao, Y.; Sirinakis, G.; Zhang, Y. Highly Anisotropic Stability and Folding Kinetics of a Single Coiled Coil Protein under Mechanical Tension. *J. Am. Chem. Soc.* **2011**, *133*, 12749. [CrossRef]

47. Gao, Y.; Zorman, S.; Gundersen, G.; Xi, Z.; Ma, L.; Sirinakis, G.; Rothman, J.E.; Zhang, Y. Single Reconstituted Neuronal SNARE Complexes Zipper in Three Distinct Stages. *Science* **2012**, *337*, 1340. [CrossRef]

48. Yu, H.; Guptaa, A.N.; Liua, X.; Neupanea, K.; Brigleyb, A.M.; Sosovab, I.; Woodside, M.T. Energy landscape analysis of native folding of the prion protein yields the diffusion constant, transition path time, and rates. *Proc. Natl. Acad. Sci. USA* **2012**, *109*, 14452. [CrossRef]

49. Hummer, G.; Szabo, A. Kinetics from Nonequilibrium Single-Molecule Pulling Experiments. *Biophys. J.* **2003**, *85*, 5–15. [CrossRef]

50. Dudko, O.K.; Hummer, G.; Szabo, A. Intrinsic Rates and Activation Free Energies from Single-Molecule Pulling Experiments. *Phys. Rev. Lett.* **2006**, *96*, 108101. [CrossRef]

51. Bustamante, C.; Marko, J.; Siggia, E.; Smith, S. Entropic elasticity of lambda-phage DNA. *Science* **1994**, *265*, 1599–1600. [CrossRef]

52. Viader-Godoy, X.; Manosas, M.; Ritort, F. Sugar-Pucker Force-Induced Transition in Single-Stranded DNA. *Int. J. Mol. Sci.* **2021**, *22*, 4745. [CrossRef] [PubMed]

53. Alemany, A.; Ritort, F. Determination of the elastic properties of short ssDNA molecules by mechanically folding and unfolding DNA hairpins. *Biopolymers* **2014**, *101*, 1193–1199. [CrossRef]

54. Makarov, A.A.; Protasevich, I.I.; Kuznetsova, N.V.; Fedorov, B.B.; Korolev, S.V.; Struminskaya, N.K.; Bazhulina, N.P.; Leshchin-skaya, I.B.; Hartley, R.W.; Kirpichnikov, M.P.; et al. Comparative Study of Thermostability and Structure of Close Homologues—Barnase and Binase. *J. Biomol. Struct. Dyn.* **1993**, *10*, 1047–1065. [CrossRef] [PubMed]

55. Griko, Y.V.; Makhatadze, G.I.; Privalov, P.L.; Hartley, R.W. Thermodynamics of barnase unfolding. *Protein Sci.* **1994**, *3*, 669–676. [CrossRef] [PubMed]

56. Galano-Frutos, J.J.; Sancho, J. Accurate Calculation of Barnase and SNase Folding Energetics Using Short Molecular Dynamics Simulations and an Atomistic Model of the Unfolded Ensemble: Evaluation of Force Fields and Water Models. *J. Chem. Inf. Model.* **2019**, *59*, 4350–4360. [CrossRef] [PubMed]

57. Hyeon, C.; Thirumalai, D. Forced-Unfolding and Force-Quench Refolding of RNA Hairpins. *Biophys. J.* **2006**, *90*, 3410–3427. [CrossRef]

58. Manosas, M.; Collin, D.; Ritort, F. Force-Dependent Fagility in RNA hairpins. *Phys. Rev. Lett.* **2006**, *96*, 218301. [CrossRef]

59. Alemany, A.; Ritort, F. Force-Dependent Folding and Unfolding Kinetics in DNA Hairpins Reveals Transition-State Displacements along a Single Pathway. *J. Phys. Chem. Lett.* **2017**, *8*, 895–900. [CrossRef]

60. Matouschek, A.; Fersht, A. Applications of physical organic chemistry to engineered mutants of barnase: Hammond postulate behaviour in the transition state of protein folding. *Proc. Natl. Acad. Sci. USA* **1993**, *90*, 7814. [CrossRef]

61. Waite, J. 11-Quinone-Tanned Scleroproteins. In *Metabolic Biochemistry and Molecular Biomechanics*; Hochachka, P.W., Ed.; Academic Press: Cambridge, MA, USA, 1983; pp. 467–504. [CrossRef]

62. Lu, Y.; Yeung, N.; Sieracki, N.; Marshall, N.M. Design of functional metalloproteins. *Nature* **2009**, *460*, 855–862. [CrossRef] [PubMed]

63. Hayashi, S.; Wu, H.C. Lipoproteins in bacteria. *J. Bioenerg. Biomembr.* **1990**, *22*, 451–471. [CrossRef] [PubMed]